23. Hsieh, C.-L. *In vivo* activity of murine *de novo* methyltransferases, Dnmt3a and Dnmt3b. *Mol. Cell. Biol.* (in the press).
24. Jeddeloh, J. A., Stokes, T. L. & Richards, E. Maintenance of genomic methylation requires a SWI2/SNF2-like protein. *Nature Genet.* **22,** 94–97 (1999).
25. Brown, K. E. *et al.* Association of transcriptionally silent genes with Ikaros complexes at contromeric heterochromatin. *Cell* **91,** 845–854 (1997).
26. Chen, R. Z., Petterson, U., Beard, C., Jackson-Grusby, L. & Jaenisch, R. DNA hypomethylation leads to elevated mutation rates. *Nature* **395,** 89–93 (1998).
27. Bestor, T. H. The host defence function of genomic methylation patterns. *Novartis Found. Symp.* **214,** 187–195 (1998).
28. Hsieh, C.-L. Dependence of transcriptional repression on CpG methylation density. *Mol. Cell. Biol.* **14,** 5487–5494 (1994).
29. Reynaud, C. *et al.* Monitoring of urinary excretion of modified nucleosides in cancer patients using a set of six monoclonal antibodies. *Cancer Lett.* **61,** 255–262 (1992).

Acknowledgements

We thank members of the European ICF Consortium for providing patient materials; B. F. Erlanger for discussions; E. Li for providing cDNA clone pMT3B for mouse Dnmt3B; B. Tycko for DNA samples; L. Nickelsen for technical assistance; K. Anderson for comments on the manuscript; and A. Niveleau for monoclonal antibody to m^5C. Supported by grants from the NIH and the Leukemia Society of America (T.H.B.) and the Danish Research Councils and the Danish Cancer Society (N.T.).

Correspondence and requests for materials should be addressed to T.H.B. (e-mail: THB12@columbia.edu).

A plant regulator controlling development of symbiotic root nodules

Leif Schauser, Andreas Roussis, Jiri Stiller* & Jens Stougaard

Laboratory of Gene Expression, Department of Molecular and Structural Biology, University of Aarhus, Gustav Wieds Vej 10, 8000 Aarhus C, Denmark

Symbiotic nitrogen-fixing root nodules on legumes are founded by root cortical cells that de-differentiate and restart cell division to establish nodule primordia. Bacterial microsymbionts invade these primordia through infection threads laid down by the plant and, after endocytosis, membrane-enclosed bacteroids occupy cells in the nitrogen-fixing tissue of functional nodules. The bacteria excrete lipochitin oligosaccharides[1,2], triggering a developmental process that is controlled by the plant and can be suppressed. Nodule inception initially relies on cell competence in a narrow infection zone located just behind the growing root tip. Older nodules then regulate the number of nodules on a root system by suppressing the development of nodule primordia[3]. To identify the regulatory components that act early in nodule induction, we characterized a transposon-tagged *Lotus japonicus* mutant, *nin* (for nodule inception), arrested at the stage of bacterial recognition. We show that *nin* is required for the formation of infection threads and the initiation of primordia. NIN protein has regional similarity to transcription factors, and the predicted DNA-binding/dimerization domain identifies and typifies a consensus motif conserved in plant proteins with a function in nitrogen-controlled development.

Inoculation of *L. japonicus*[4] roots with *Mesorhizobium loti* bacteria results in the development of functional root nodules. The nitrogen reduced by the bacteroids in the infected nodule cells allows the plants to grow in the absence of a nitrogen source, such as nitrate (see refs 5, 6) (Fig. 1a). This provides conditions for a mutant screen in which mutants with ineffective symbiosis have a short stature, light-green chlorotic leaves and red stem pigmentation resulting from nitrogen starvation. Inoculated *nin* mutants did not develop nodules (Fig. 1b) and were therefore easily identified in a screen for transposon-tagged symbiotic mutants. After being transferred to nitrogen-containing nutrients, the *nin* mutants resumed growth. We did not observe any morphological change to the roots, shoots, leaves, flowers or seeds, indicating that *Nin* may not be required for general plant development.

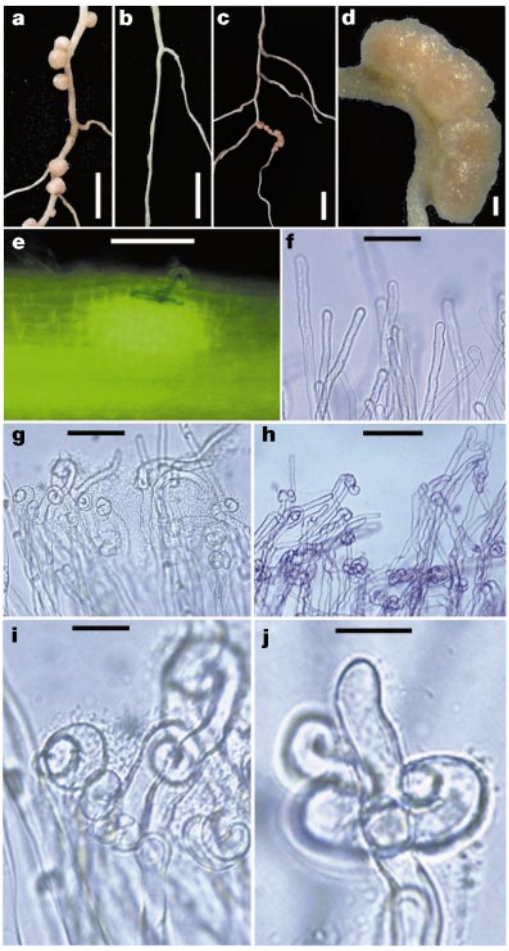

Figure 1 The phenotype of *nin* non-nodulating mutants. **a**, Wild-type root nodules. **b**, Non-nodulating *nin* phenotype. **c**, Nodulated revertant sector on an unstable *nin-1* mutant. **d**, Close up of a small revertant sector. **e**, Fluorescence microscopy of infection thread and nodule primordium on a wild-type plant. **f**, Light microscopy of root hairs on a *nin* mutant inoculated with the *nodC::Tn5* bacterial mutant. **g**, Root-hair curling in the wild type. **h**, Root-hair deformation and curling on a *nin* mutant. **i**, 'Shepherd's crook' in the wild type. **j**, Curling and deformation on a *nin* mutant. Scale bars: **a–c**, 1 cm; **d**, 1 mm; **e**, 0.9 mm; **f**, 50 μm; **g**, 70 μm; **h**, 100 μm; **i**, **j**, 20 μm.

To establish when and where *Nin* acts during nodule development, bacterial invasion was visualized by staining for β-galactosidase activity expressed from a *hemA–lacZ* reporter in *M. loti*. An infection thread passing through a root hair towards the dividing cells of a wild-type plant is shown in Fig. 1e. Neither infection threads nor nodule primordia were observed in the *nin* mutants. Moreover, the first formative cell divisions in the outer cortex were not observed by light or fluorescence microscopy of *nin* mutants (not shown). After recognizing the microsymbiont, wild-type plants respond by curling root hairs to form the infection pockets of the infection zone (Fig. 1g, i). In *nin* mutants, normal curling into 'shepherd's crook' structures was accompanied by excessive deformation or curling of individual root hairs (Fig. 1h, j). In a plate inoculation system, the infection zone defined by root-hair curling covered ~2 mm in wild-type plants, compared with

* Present address: Plant Molecular Genetics, University of Tennessee, Knoxville, Tennessee 37901-1071, USA.

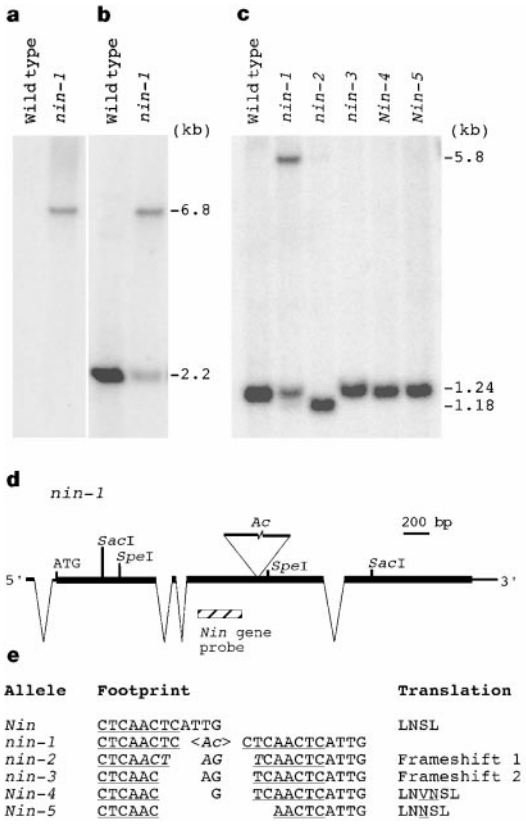

Figure 2 Structure of the *Nin* gene and the allelic series derived by *Ac* transposition. **a**, Southern hybridization with an *Ac* probe visualizes the 6.8-kb *Sac*I fragment in *nin-1* mutants. **b**, *Nin* gene probe visualizes the 6.8-kb *Sac*I fragment and the wild-type 2.2-kb *Sac*I fragment originating from somatic excision in *nin-1* mutants. **c**, *Spe*I RFLP after *Ac* excision in the *nin-2* allele; gene probe hybridization. **d**, Primary structure of the *Nin* gene and position of the *Ac* insertion in the *nin-1* allele. **e**, The insertion site sequence (underlined) and the *Ac* footprints detected in genetically stable mutants and germinal revertants.

~8 mm towards the tip of *nin* mutant roots (not shown). Inoculation with a *M. loti nodC::Tn5* mutant unable to synthesize lipochitin oligosaccharides triggered no deformation or curling on wild-type plants or *nin* mutants (Fig. 1f). This dependence on lipochitin oligosaccharides was verified by application of purified *M. loti* lipochitin oligosaccharides[7]. Root-hair deformation was observed on both the wild-type plants and the *nin* mutants. We conclude from these observations that perception of the lipochitin oligosaccharide signal is functional in root hairs of *nin* mutants and that the non-nodulating phenotype of *nin* mutants is caused by developmental arrest or a signal-transduction defect before the initiation of infection threads and extensive cell division in the cortical cells. Negative regulation of root-cell competence in wild-type plants is suggested by the extended infection zone on *nin* mutants.

We identified the monogenic recessive *nin* mutant locus in a screening for symbiotic mutants carrying the autonomous maize transposon *Ac*. When mutant offspring were rescreened to test the stability of the mutation, phenotypic reversion was observed on 10–15% of progeny. Sectors of active pink nodules on the roots indicated somatic reversions due to *Ac* excision and the restoration of gene function (Fig. 1c, d). Densely packed nodules developing in small revertant sectors all appeared to be at roughly the same developmental stage and sector boundaries were well defined (Fig. 1c, d), indicating that *Nin* acts locally and not systemically.

Southern-blot analysis of mutant plants identified a common transposed *Ac* element, shown by the 6.8-kilobase (kb) *Sac*I fragment in Fig. 2a, b. In 50 normal and mutant T2 plants, this transposed *Ac* cosegregated with unstable mutant alleles present in heterozygotes and mutants, whereas it was absent in homozygous wild-type siblings and stable mutants. We used the transposon tag to isolate and subsequently sequence the *Nin* gene. In unstable mutants, a *Nin* gene probe (Fig. 2d) was used to detect the restriction fragment length polymorphism (RFLP) produced by an *Ac* (4.65 kb) insertion in the wild-type 2.2-kb *Sac*I fragment (Fig. 2b). This RFLP was absent in wild-type plants, in two stable mutants, and in 12 stable germinal revertants. The *Ac*-tagged

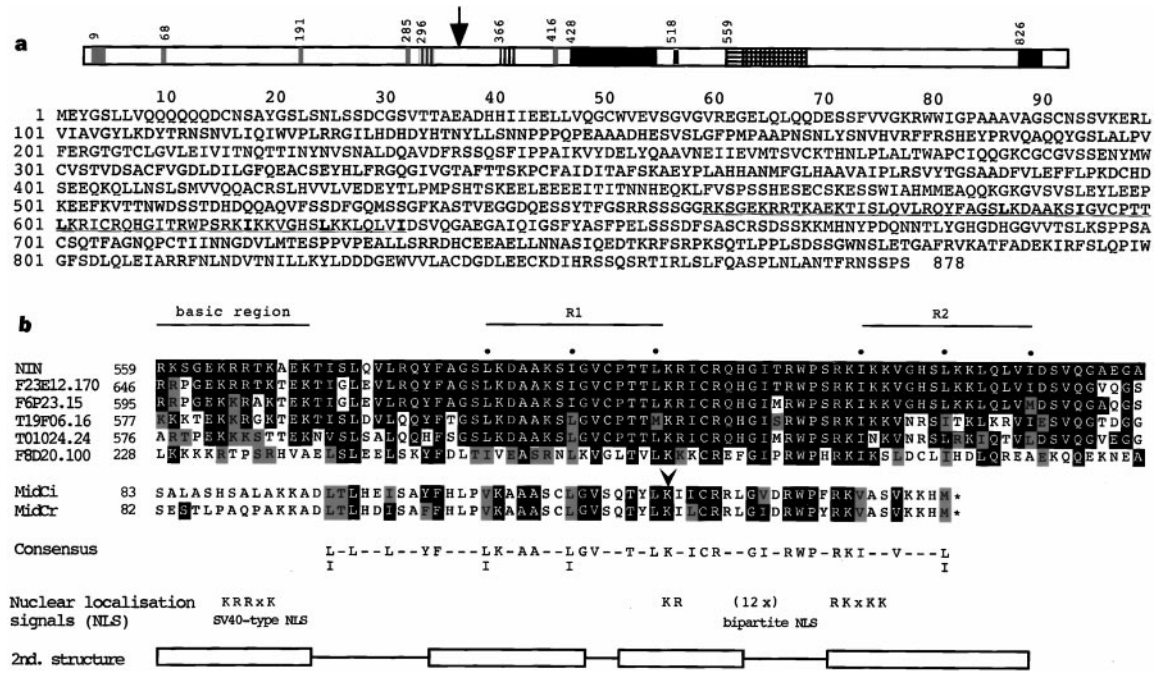

Figure 3 Amino-acid sequence and domains of NIN protein. **a**, Sequence of the 878-amino-acid protein. The basic R1/R2 region is underlined and the leucine/isoleucine heptad repeats are in bold. The position of the putative membrane-spanning regions and activation domains are shown, and an arrow indicates the *Ac* integration site. Grey, glutamine hexamer and dimers; vertical hatching, membrane-spanning segments; black, acidic domains; horizontal hatching, basic region; cross-hatching, heptad repeat region. **b**, Alignment to the similar *Arabidopsis* proteins and the C terminus of the *Chlamydomonas* Mid proteins. Dots indicate heptad repeats; arrowhead indicates the K124 of Mid. Nuclear localization signals are shown. Helix predictions for NIN are shown as open boxes. Amino acids identical to NIN are shown on a black background and conservative changes on grey. The consensus includes amino acids, conserved in six or more proteins and I/L substitutions.

unstable mutant allele was designated *nin-1*. The structure of *Nin* and the position of *Ac* in exon 4 of the *nin-1* allele are shown in Fig. 2d.

In the *nin-1* allele, the *Ac* element was flanked by the characteristic 8-base pair (bp) direct repeat of the target insertion sequence (Fig. 2e). Excision of *Ac* creates small sequence alterations at the integration site. These 'footprints' were amplified using the polymerase chain reaction and were determined in 12 independent genetically stable revertants and two stable mutants. The stable mutant alleles *nin-2* and *nin-3* revealed sequence alterations causing translational frameshifts (Fig. 2e). In the *nin-2* allele, the footprint creates a *Spe*I restriction site and the RFLP seen in Fig. 2c. The footprints of the stable revertant alleles *Nin-4* and *Nin-5* translate into two and one additional amino acids, respectively (Fig. 2e). The wild-type sequence was found in 10 stable revertants. This allelic series with *Ac* in the unstable *nin-1* allele, footprints leading to stable frameshift mutations, and restoration of the reading frame in germinal revertants, demonstrates that the non-nodulating *nin* mutation was caused by insertion of the *Ac* element.

To further investigate the role of *Nin* in the molecular mechanisms governing nodule organogenesis, a complementary DNA was isolated and the structure of the derived protein analysed. The full-length *Nin* cDNA has an open reading frame of 2,634 bp, a 5′ leader with stop codons in all three reading frames, and a 3′ untranslated region of 141 bp. The protein, comprising 878 amino acids, is shown in Fig. 3a along with a diagram of several domains with similarity to transcription factors. The carboxy-terminal half of the protein carries an unusual putative DNA-binding domain with a basic region followed by two heptad leucine or isoleucine repeats (R1 and R2); an amphiphatic leucine-zipper structure was predicted for R2 by helical-wheel analysis (Fig. 3). This arrangement is similar to the DNA-binding/dimerization domains of the bZIP[8] and bHLH/Z[9] transcription factors, but the R1/R2 region does not comply with a strict consensus of either domain. The distance between the basic region and the zipper, for example, is longer than would be expected from the bZIP consensus. The presence of a proline helix breaker (Pro 597) in R1 also distinguishes NIN, and alignment to prokaryotic helix–turn–helix DNA-binding domains[10] suggests a GV turn motif preceding Pro 597 (not shown). No known DNA-binding/dimerization domains combine these components, and the structure of the domain has yet to be resolved by crystallography. Two acidic domains located between residues 428–503 and 826–845 may function as transcriptional activation domains. Supporting the role as a transcription factor, NIN has SV40-like and bipartite nuclear localization signals[11] (Fig. 3). Less clear is the role of a hexaglutamine stretch between residues 9–14 and five double and eight single glutamine residues within the first 420 amino acids.

Two membrane-spanning segments were predicted for NIN (Fig. 3a). One of these segments has similarity to previously assigned membrane-spanning regions in the *Rickettsia prowazekii* ATP/ADP translocase[12] and in the photosystem I apoprotein A1 (ref. 13). The significance of the NIN segments is supported by the prediction of similarly positioned membrane helices in two *Arabidopsis* orthologues. These segments may alternatively constitute hydrophobic domains in the folded proteins.

The crucial role of *Nin* during nodulation may be taken to indicate that this gene was maintained only in legumes to serve this particular developmental process. This is not the case, however, as BLAST searches identified four similar *Arabidopsis* genes (F23E12.170, F6P23.15, T19F06.16 and T01024.24) of unknown function. In the translation products there is a remarkable conservation of the NIN putative DNA-binding domain (Fig. 3b), although other regions are less conserved. Further evidence of this region having an unusual structure comes from comparison of NIN and the four *Arabidopsis* proteins to the protein translated from the *Arabidopsis* F8D20.100 gene and the Minus dominance (Mid) proteins from *Chlamydomonas*[14]. This comparison defines a short consensus for these otherwise diverse proteins (Fig. 3b). Because the most striking feature is the invariant RWPxRK motif, we tentatively call this structure the RWP–RK domain. Its importance was demonstrated by a mutation changing the consensus Lys 124 to isoleucine[14], which inactivated the Mid protein.

The regional similarity observed between NIN and the Mid proteins of *Chlamydomonas*[14,15] (Fig. 3b) may have functional significance. In *Chlamydomonas*, Mid is encoded in the mating-type locus and determines the development of minus gametes during gametogenesis. The *mid* gene controls the expression of *minus*-specific genes and represses the expression of the opposing *plus*-specific genes. It functions as a developmental regulator gene and is both necessary and sufficient to determine the mating type of *Chlamydomonas* cells[14]. Gametogenesis in *C. reinhardtii* is induced by nitrogen limitation[16], which is also a prerequisite not only for root nodule initiation but also to prevent the suppression of nodule

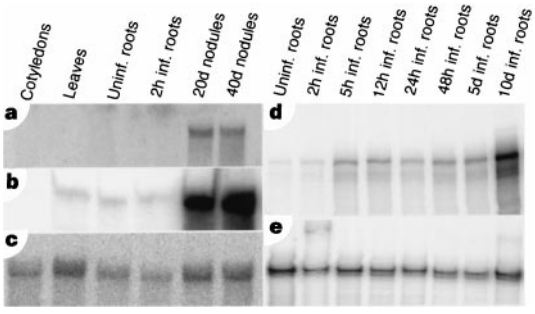

Figure 4 Expression of *Nin* during root-nodule development. **a**, **b**, *Nin* expression obtained by northern hybridization (**a**) and RNase protection studies (**b**) of different plant organs. **c**, Northern hybridization of Ubiquitin control. **d**, RNase protection showing *Nin* gene expression in root tissue after inoculation with *M. loti*. **e**, Ubiquitin control RNase protection. Time after infection (inf.) is shown in hours (h) or days (d).

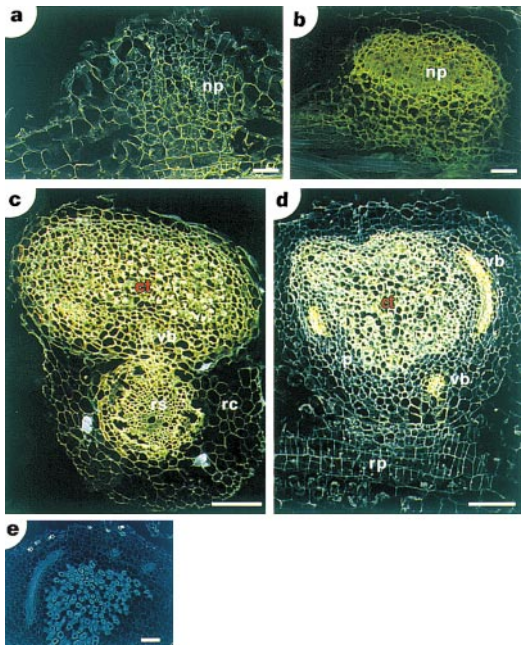

Figure 5 *In situ* localization of the *Nin* transcripts during nodule development. **a**, Early stage of module primordium with low-level *Nin* expression in dividing cells. **b**, Nodule primordium at a later stage expressing *Nin* at higher level. **c**, Transverse nodule section showing *Nin* expression in the central tissue, vascular bundles and root stele. **d**, Fully differentiated nitrogen-fixing nodule. *Nin* expression is confined to vascular bundles, parenchyma, and infected and uninfected cells of the central tissue. **e**, Sense control. Abbreviations: np, nodule primordium; ct, central tissue; rc, root cortex; rs, root stele; vb, vascular bundle. Scale bar, 100 μm.

development. The similarity between NIN and Mid is remarkable because the *Chlamydomonas mid* gene has undergone rapid evolution, and conservation was detected only between the closely related *C. reinhardtii* and *C. incerta*[15].

The phenotype of the *nin* mutants indicates that *Nin* is involved in the inception of root nodules, and the features of NIN the protein suggest that it acts as a transcriptional regulator of genes required for nodule development. To determine the developmental stage and cell types in which *Nin* may be involved in the transcriptional regulation of downstream genes, we investigated *Nin* expression by northern hybridization, RNase protection and *in situ* localization. The highest number of transcripts was found in young pink nodules (20 days after infection) and mature nodules (40 days). Some steady-state messenger RNA was detected in cotyledons, leaves, stems and roots by the more sensitive RNase protection assay (Fig. 4a, b, c). The size of the *Nin* transcript was found to be approximately 3,000 nucleotides, corresponding to the 2,888-bp cDNA plus a poly(A) tail. To follow the kinetics of *Nin* expression, we determined the level of steady-state messenger RNA during early phases of nodule initiation, when root and nodule tissue cannot be analysed separately (Fig. 4d, e). A marginal upregulation was detected 5 h after infection, followed by a substantial increase 10 days after infection, when small nodules were clearly visible. *In situ* hybridization with antisense digoxigen-labelled riboprobes was used to visualize the cellular expression pattern. In the developing nodules, transcripts were detected in the primordium cells (Fig. 5a, b, e). Later in nodule development, *Nin* expression was localized to the nodule parenchyma, the nodule vascular bundles, and the uninfected and infected cells of the central tissue (Fig. 5c, d), but was not detected or was significantly lower in the nodule and root cortex. In transverse sections, *Nin* transcripts were localized in root vascular tissue (Fig. 5c). This expression pattern shows that transcriptional regulation of *Nin* directs expression to certain cell types and that expression is not organ specific. Expression of *Nin* in mature nodules indicates that it may be involved not only during nodule inception, but also later during nodule development.

The lipochitin oligosaccharide-dependent root-hair curling and extensive root-hair deformation indicate that the perception of lipochitin oligosaccharide is at least partly functional in the *nin* mutants. The competence of the root hair cells in the infection zone and the recognition and early interaction with the microsymbiont therefore seem to be unaffected. These findings place *Nin* in the signal perception–transduction or gene-activation pathway downstream of the early signal exchange between the symbionts. Further experiments are required to establish the exact function, but the structure of NIN points towards a role in gene activation. The presence of putative membrane-spanning helices in NIN is reminiscent of the membrane-bound SREBP and Notch regulators. In humans, the SREBP proteins, which regulate the transcription of genes involved in cholesterol uptake and biosynthesis, are bound to the membrane of the nucleus and endoplasmic reticulum[17]. A two-step proteolytic cleavage involving an activation protein and a peptidase[18,19] releases the bHLH/Z transcriptional activator under sterol depletion. Cell-fate determination in *Drosophila*, determined by the Notch transmembrane receptor, is another example of signalling mediated by proteolytic cleavage. Ligand binding at the extracellular domain induces the release of the intracellular domain, which enters the nucleus as a transcriptional co-regulator[20]. Similarly, the membrane-spanning regions suggested for NIN raise the possibility of post-translational control, and a model for the role and regulation of *Nin* can be summarized as follows. Membrane-bound NIN in target cells is proteolytically cleaved, and relocalization of the C-terminal transcriptional regulator peptide to the cell nucleus allows a quick response to the signal transduction triggered by bacterial infection. Transcriptional activation of *Nin* takes place simultaneously in the dividing cells. Downstream genes are then activated and the nodule primordia are established. Another *Nin*-dependent signal promotes the growth of infection threads and negatively regulates root-hair competence. Absence of this signal in mutants leads to the lack of infection thread, excessive root-hair response and expansion of the infection zone seen in *nin* plants.

The nitrogen regulation of nodule organogenesis and *Chlamydomonas* gametogenesis together with the conserved domain embedding the RWP–RK motif of NIN and Mid indicate that this domain is involved in the regulation of genes controlled by nitrogen status. Because the conserved domain was found only in proteins from algae and higher plants, this class of regulator proteins probably evolved after the common ancestor of algae and plants diverged from the other eukaryotes.

Methods

Plant material

The *Ac* transposon approach has been described[21] and the screening conditions for nodulation with *M. loti* strain NZP2235 were as previously outlined[22]. The *nin* mutants were found in progeny from a T1 plant during a screen for symbiotic mutants segregating from 100 primary transformants carrying *Ac* launching constructs. The T2 segregation ratio was 644 wild type: 179 *nin* mutants. Homozygous and heterozygous plants confirming the recessive inheritance were identified after screening progeny from T2 and T3 plants. The *nin* mutant phenotype was tested and confirmed with another *M. loti* strain, R7A[23].

Microscopy

Plants were inoculated with *M. loti* NZP2235 carrying a *hemA–lacZ* reporter construct. Entire roots were stained for *lacZ* activity[24], cleared in lactic acid and observed under an Axioscope microscope (Zeiss) with bright field or fluorescence. The *nodC::Tn5* strain is an R7A derivative.

Cosegregation analysis

DNA from mutant and normal siblings was digested and transferred to nylon membranes. The radioactive *Nin* gene probe was prepared by labelling of a PCR fragment using the Random Primed Kit (Boehringer Mannheim).

Isolation of flanking regions

The plant DNA flanking the left end of *Ac* in the *Nin-1* allele was isolated by inverse PCR[25] using the *Ac* primers 5′-CGACTTTAACCCGACCGATCCTATCGG-3′ and 5′-GCAAGGCGCATGCATCAAAACAAGGCG-3′. Plant DNA flanking the right end was amplified using the *Ac* primer 5′-GTAGAGCTAGTTTCCCGACCGTTTCACC-3′ and a primer 5′-CCTCCATCATGTGTGCAATCCATG-3′ derived from the cDNA. The DNA-extraction procedure has been described[22]. *Ac* excision footprints were obtained using the *Nin* gene-specific primers 5′-CAAGGAATTGTTGGTACAGCCTTC-3′ and 5′-CCTCCATCATGTGTGCAATCCATG-3′ flanking the *Ac* element. PCR fragments of 550 bp were sequenced.

cDNA isolation

The *Nin* gene probe was used to screen 700,000 plaque-forming units of an unamplified oligo dT-primed nodule cDNA library. One hybridizing clone of 2,541 bp was found. The full-length cDNA was assembled by adding 304 bp isolated from a random-primed nodule cDNA library. 5′ Rapid amplification of cDNA ends was used to map the transcription start sites corresponding to transcripts of 2,863 and 2,907 nucleotides.

In situ hybridization and RNA analysis

Ribonuclease protection assays were according to Ambion RPAII(TM) and MAXI-script(TM). A *L. japonicus* 0.26-kb ubiquitin fragment was used for normalization. A 0.6-kb *Nin* 5′ fragment was subcloned into pBluescript to provide templates for T3 and T7 polymerase transcription of sense and antisense DNA. Digoxigenin labelling of RNA probes, tissue preparation and *in situ* hybridization were as described[26]. Images were processed by using Photoshop 4.0 for presentation.

Computer analysis of sequence data

Databases were searched with BLAST (http://www.ncbi.nlm.nih.gov/) and secondary protein structures were predicted by PredictProtein (http://www.embl-heidelberg.de/). Membrane-spanning regions were predicted by SBASE (http://base.icgeb.trieste.it/), TMPRED (http://www.ch.embnet.org/), TopPred II (http://www.biokemi.su.se) and PredictProtein.

Received 19 May; accepted 26 August 1999.

1. Truchet, G. *et al.* Sulphated lipo-oligosaccharide signals of *Rhizobium meliloti* elicit root nodule organogenesis in alfalfa. *Nature* **351,** 670–673 (1991).
2. Spaink, K. *et al.* A novel highly unsaturated fatty acid moiety of lipo-oligosaccharide signals determines host specificity of *Rhizobium*. *Nature* **354,** 125–130 (1991).
3. Caetano-Anollés, G. & Gresshoff, P. M. Plant genetic control of nodulation. *Annu. Rev. Microbiol.* **45,** 345–382 (1991).
4. Handberg, K. & Stougaard, J. *Lotus japonicus*, an autogamous, diploid legume species for classical and molecular genetics. *Plant J.* **2,** 487–496 (1992).

5. Spaink, H. P., Kondorosi, A. & Hooykaas, P. J. J. (eds) *The Rhizobiaceae* (Kluwer, Dordrecht, 1998).
6. Long, S. R. *Rhizobium* symbiosis: Nod factors in perspective. *Plant Cell* **8,** 1885–1898 (1996).
7. López-Lara, I. M. *et al.* Structural identification of the lipo-chitin oligosaccharide nodulation signals of *Rhizobium loti*. *Mol. Microbiol.* **15,** 627–638 (1995).
8. Landschulz, W. H., Johnson, P. F. & McKnight, S. L. The leucine zipper: A hypothetical structure common to a new class of DNA binding proteins. *Science* **240,** 1759–1764 (1988).
9. Ferré-D'Amaré, A. R., Prendergast, G. C., Ziff, E. B. & Burley, S. K. Recognition by Max of its cognate DNA through a dimeric b/HLH/Z domain. *Nature* **363,** 38–45 (1993).
10. Puyet, A., Ibanez, A. M. & Espinosa, M. Characterisation of the *Streptococcus pneumoniae* maltosaccharide MalR, a member of the LacI-GalR family of repressors displaying distinctive genetic features. *J. Biol. Chem.* **268,** 25402–25408 (1993).
11. Silver, P. A. How proteins enter the nucleus. *Cell* **64,** 489–497 (1991).
12. Plano, G. V. & Winkler, H. H. Identification and initial topological analysis of the *Rickettsia prowazekii* ATP/ADP translocase. *J. Bacteriol.* **173,** 3389–3396 (1991).
13. Lehmbeck, J. *et al.* Sequence of two genes in pea chloroplast DNA coding for 84 and 82 kD polypeptides of the photosystem I complex. *Plant Mol. Biol.* **7,** 3–10 (1986).
14. Ferris, P. J. & Goodenough, U. W. Mating type in *Chlamydomonas* is specified by *mid*, the Minus-dominance gene. *Genetics* **146,** 859–869 (1997).
15. Ferris, P. J., Pavlovic, C., Fabry, S. & Goodenough, U. W. Rapid evolution of sex-related genes in *Chlamydomonas*. *Proc. Natl Acad. Sci. USA* **94,** 8634–8639 (1997).
16. Beck, C. F. & Haring, M. A. Gametic differentiation of *Chlamydomonas*. *Int. Rev. Cytol.* **168,** 259–302 (1996).
17. Yokoyama, C. *et al.* SREBP-1, a basic-helix-loop-helix-leucine zipper protein that controls transcription of the low density lipoprotein receptor gene. *Cell* **75,** 187–197 (1993).
18. Brown, M. S. & Goldstein, J. L. The SREBP pathway: Regulation of cholesterol metabolism by proteolysis of a membrane-bound transcription factor. *Cell* **89,** 331–340 (1997).
19. Sakai, J. *et al.* Molecular identification of the sterol-regulated luminal protease that cleaves SREBPs and controls lipid composition of animal cells. *Mol. Cell* **2,** 505–514 (1998).
20. Schroeter, E. H., Kisslinger, J. A. & Kopan, R. Notch-1 signalling requires ligand-induced proteolytic release of intracellular domain. *Nature* **393,** 382–386 (1998).
21. Thykjaer, T., Stiller, J., Handberg, K., Jones, J. & Stougaard, J. The maize transposable element *Ac* is mobile in the legume *Lotus japonicus*. *Plant Mol. Biol.* **27,** 981–993 (1995).
22. Schauser, L. *et al.* Symbiotic mutants deficient in nodule establishment identified after T-DNA mutagenesis of *Lotus japonicus*. *Mol. Gen. Genet.* **259,** 414–423 (1998).
23. Sullivan, J. T. *et al.* Nodulating strains of *Rhizobium loti* arise through chromosomal symbiotic gene transfer in the environment. *Proc. Natl Acad. Sci. USA* **92,** 8985–8989 (1995).
24. Boivin, C. *et al. Rhizobium meliloti* genes encoding catabolism of trigonelline are induced under symbiotic conditions. *Plant Cell* **2,** 1157–1170 (1990).
25. Earp, D. J., Lowe, B. & Baker, B. Amplification of genomic sequences flanking transposable elements in host and heterologous plants: a tool for transposon tagging and genome characterization. *Nucleic Acids Res.* **18,** 3271–3279 (1990).
26. Papadopoulou, K., Roussis, A. & Katinakis, P. Phaseolus ENOD40 is involved in symbiotic and non-symbiotic organogenetic processes: expression during nodule and lateral root development. *Plant Mol. Biol.* **30,** 403–417 (1996).

Acknowledgements

We thank C. Ronson for supplying the *M. loti nodC* mutant; H. Spaink for the purified *M. loti* lipochitin oligosaccharide; and A. Nielsen and S. Rye for assistance. This research was supported by the Danish Biotechnology Programme and the SJVF Whole Plant Physiology Initiative. J. Stiller was supported by the Danish Science Research Councils postdoc programme, and A.R. by the EU-TMR programme.

Correspondence and requests for materials should be addressed to J.S. (e-mail: stougaard@mbio.aau.dk).

The *Nin* gene sequence and cDNA sequence have been deposited in the EMBL database (accession nos AJ238956 and AJ239041, respectively).

CaMKII regulates the density of central glutamatergic synapses *in vivo*

Christopher Rongo & Joshua M. Kaplan

Department of Molecular and Cell Biology, LSA 361, University of California, Berkeley, California 94720-3200, USA

Synaptic connections undergo a dynamic process of stabilization or elimination during development, and this process is thought to be critical in memory and learning and in establishing the specificity of synaptic connections[1]. The type II calcium- and calmodulin-dependent protein kinase (CaMKII) has been proposed to be pivotal in regulating synaptic strength[2–4] and in maturation of synapses during development[5]. Here we describe how CaMKII regulates the formation of central glutamatergic synapses in *Caenorhabditis elegans*. During larval development, the density of ventral nerve cord synapses containing the GLR-1 glutamate receptor is held constant despite marked changes in neurite length. The coupling of synapse number to neurite length requires both CaMKII and voltage-gated calcium channels. CaMKII regulates GLR-1 by at least two distinct mechanisms: regulating transport of GLR-1 from cell bodies to neurites; and regulating the addition or maintenance of GLR-1 to postsynaptic elements.

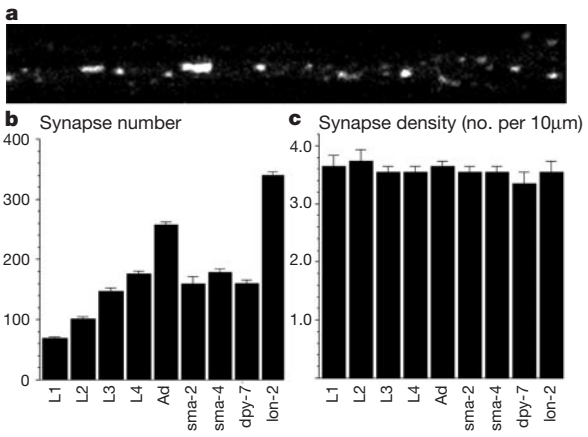

Figure 1 Formation of GLR-1::GFP clusters. **a**, GLR-1::GFP accumulates in clusters along the lengths of neurites in the ventral nerve cord. **b**, Individual GLR-1::GFP clusters in the ventral nerve cord were counted in wild-type larvae (L1–L4) and adults (Ad), as well as in mutant adults with short (*sma-2*, *sma-4* and *dpy-7*) or long (*lon-2*) body lengths. **c**, Data plotted as synaptic density (number of GLR-1::GFP clusters per 10 μm nerve cord length). Values are means ± s.e.m. Ten to thirty animals were examined for each entry.

To determine how central synapses change in number and morphology during development, we observed neuron–neuron synapses that contain the α-amino-3-hydroxy-5-methyl-4-isoxazole propionic acid (AMPA)-type glutamate receptor (GluR) GLR-1 (refs 6, 7). We previously showed that chimaeric receptors tagged with the green fluorescent protein (GLR-1::GFP) can be used to visualize central glutamatergic synapses in living animals[8]. GLR-1::GFP is localized to discrete punctate structures (Fig. 1a; hereafter called clusters) along the lengths of neurites in both the ventral cord and nerve ring processes, where the majority of interneuron synapses reside[9]. GLR-1-containing neurites extend the full length of the ventral nerve cord throughout larval and adult development; thus, these neurites must elongate as the animal grows[9]. To see how synapse numbers are affected by changes in neurite length, we examined the number of GLR-1::GFP clusters in the ventral cord during larval development (Fig. 1b). First stage (L1) larvae had ~60 clusters whereas adults had ~260 clusters in the ventral cord. This apparent increase in GLR-1-containing synapses occurs despite the fact that the number of GLR-1-expressing cells remains constant throughout larval development[6,7]. Homozygous *lin-5* mutants, which lack postembryonic cell divisions[10], have similar numbers of GLR-1::GFP clusters (193 ± 17, $n = 10$) as their age-matched (L4 stage) heterozygous siblings (181 ± 6, $n = 10$). Therefore, the GLR-1::GFP clusters added during larval development are not induced by synaptic partners produced by post-embryonic lineages. One simple model explaining these results is that developing animals maintain a constant density of GLR-1-containing synapses along the ventral cord, thereby necessitating addition of synapses to compensate for increased body length.

We tested the relationship between synapse number and body length by comparing the number of GLR-1::GFP clusters with the length of the ventral cord in developing worms. Although cluster number varies nearly fourfold from early L1 to adulthood, the density of clusters was constant throughout larval development (~3.7 per 10 μm) (Fig. 1b, c). Similarly, compensatory changes occurred in the number of GLR-1::GFP clusters in short and long